

Contents lists available at [SciVerse ScienceDirect](http://www.sciencedirect.com)

Acta Biomaterialia

journal homepage: www.elsevier.com/locate/actabiomat

Effect of biologically relevant ions on the corrosion products formed on alloy AZ31B: An improved understanding of magnesium corrosion [☆]

Yongseok Jang, Boyce Collins, Jagannathan Sankar, Yeoheung Yun ^{*}

Engineering Research Center for Revolutionizing Metallic Biomaterials (ERC-RMB), North Carolina A&T State University, Greensboro, NC 27411, USA

ARTICLE INFO

Article history:
Available online xxx

Keywords:
Biodegradable metal
Magnesium
Corrosion
Corrosion product

ABSTRACT

Simulated physiological solutions mimicking human plasma have been utilized to study the in vitro corrosion of biodegradable metals. However, corrosion and corrosion product formation are different for different solutions with varied responses and, hence, the prediction of in vivo degradation behavior is not feasible based on these studies alone. This paper reports the role of physiologically relevant salts and their concentrations on the corrosion behavior of a magnesium alloy (AZ31B) and subsequent corrosion product formation. Immersion tests were performed for three different concentrations of Ca^{2+} , HPO_4^{2-} , HCO_3^- to identify the effect of each ion on the corrosion of AZ31B assessed at 1, 3 and 10 days. Time-lapse morphological characterization of the samples was performed using X-ray computed tomography and scanning electron microscopy. The chemical composition of the surface corrosion products was determined by electron dispersive X-ray spectroscopy and X-ray diffraction. The results show that: (1) calcium is not present in the corrosion product layer when only Cl^- and OH^- anions are available; (2) the presence of phosphate induces formation of a densely packed amorphous magnesium phosphate corrosion product layer when HPO_4^{2-} and Cl^- are present in solution; (3) octacalcium phosphate and hydroxyapatite (HAp) are deposited on the surface of the magnesium alloy when HPO_4^{2-} and Ca^{2+} are present together in NaCl solution (this coating limits localized corrosion and increases general corrosion resistance); (4) addition of HCO_3^- accelerates the overall corrosion rate, which increases with increasing bicarbonate concentration; (5) the corrosion rate decreases due to the formation of insoluble HAp on the surface when HCO_3^- , Ca^{2+} , and HPO_4^{2-} are present together.

© 2013 Acta Materialia Inc. Published by Elsevier Ltd. All rights reserved.

1. Introduction

Biodegradability and similar mechanical properties to human bone make magnesium a promising candidate for implantable materials used in medical devices. Recent efforts to develop more biocompatible metallic implants have focused not only on magnesium alloy design to match the engineering requirements demanded of medical devices [1–3], but also on understanding the degradation behavior in specific biomedical application environments [4–7]. The biodegradation of metallic magnesium is fundamentally linked to studies of its “corrosion”, which is dependent on the interface dynamics between the material and its environment. Identifying and understanding the biological and material factors that govern the corrosion kinetics and mechanisms are of prime importance to the successful development of biodegradable implants.

Currently, applying in vitro test results generated using simulated body fluids (SBFs) to predict in vivo degradation behavior is unreliable because factors affecting the complex biomedical environment, such as the concentrations of salts, flow dynamics, protein absorption and active tissue formation, cannot be replicated solely by immersion in SBFs. Previous studies have used various solutions, such as NaCl solution [8,9], Hank’s balanced salt solution [10,11], SBF [12–14] and Dulbecco’s modified Eagle’s medium (DMEM) [15,16] to study the corrosion behavior of magnesium alloys. Additionally, the effect of different inorganic ions, such as Cl^- [13,17,18], Ca^{2+} [13], HCO_3^- [17–20], and HPO_4^{2-} [13,18,21], have been investigated. However, the mechanism(s) of corrosion and corrosion product formation upon exposure to individual ions combined with salts and their concentrations is not well established.

This paper is an attempt to identify the effects of biologically relevant salts and their concentrations on the corrosion behavior and corrosion product formation using the standard immersion test. It is thought that this fundamental understanding of in vitro corrosion studies will ultimately provide a basis for comparison

[☆] Part of the Biodegradable Metals Conference 2012 Special Issue, edited by Professor Frank Witte and Professor Diego Mantovani.

^{*} Corresponding author. Tel.: +1 336 256 1151.

E-mail address: yyun@ncat.edu (Y. Yun).

Table 1
The ionic composition and concentration of each test solution and blood plasma.

Concentration (mmol l ⁻¹)	Na ⁺	K ⁺	Ca ²⁺	Mg ²⁺	Cl ⁻	HCO ₃ ⁻	HPO ₄ ²⁻	SO ₄ ²⁻
Blood plasma [22]	142.0	5.0	2.5	1.5	103.0	27.0	1.0	0.5
Solution 1	103.0				103.0			
Solution 2	102.0		0.5		103.0			
Solution 3	98.0		2.5		103.0			
Solution 4	83.0		10.0		103.0			
Solution 5	103.4				103.0		0.2	
Solution 6	105.0				103.0		1.0	
Solution 7	113.0				103.0		5.0	
Solution 8	103.5				103.0	0.5		
Solution 9	130.0				103.0	27		
Solution 10	153.0				103.0	50		
Solution 11	100.0		2.5		103.0		1.0	
Solution 12	127.0		2.5		103.0	27	1.0	

with results from in vivo studies while isolating and characterizing the corrosion products associated with the biodegradation process.

2. Materials and methods

Cylindrical specimens 6.35 mm in diameter and 2 mm high were cut from a rod of as-drawn AZ31B magnesium alloy (Goodfellow Corp., USA), polished with up to 1200 grit silicon carbide sand, and cleaned with acetone and ethyl alcohol. The final height was adjusted to 1.3 mm after polishing.

Immersion tests were carried out in the various solutions shown in Table 1, in an Isotemp incubator (model No. 1602D Fisher Scientific, USA) at 37 °C for 1, 3 and 10 days to compare corrosion in each solution. The solutions were prepared with salt concentrations relevant to those found in blood plasma (Table 1) [22]. Solution 1 was a NaCl solution with a similar concentration of Cl⁻ to that of blood plasma. This concentration of Cl⁻ ions was common to all solutions. The Ca²⁺ concentration in solutions 2–4 was varied based on the concentration in blood plasma. In the same way, solutions 5–7 contained varying amounts of HPO₄²⁻, and solutions 8–10 varying amounts of HCO₃⁻. The types of salts present in solutions 11 and 12 were varied. These solutions were made with NaCl, CaCl₂, Na₂HPO₄·7H₂O and NaHCO₃. The ratio of volume of solution to sample was 330 ml cm⁻² and the initial pH of the solutions was adjusted to 7.4 ± 0.05. The solutions were changed every day to minimize the influence of pH.

The pH of the solutions was measured with a pH meter (Oakton® pH2100, Eutech Instruments, Singapore) before changing the solution. The outward appearance and cross-sectional images of the samples after immersion for 10 days were observed using

a digital camera and by micro-CT (Phoenix Nanotom-M™, GE Sensing & Inspection Technologies GmbH, Germany). X-ray emission parameters were 80 kV and 180 μA and the number of projections acquired (*N_p*) was 1800. The PCA file format (Phoenix CT Acquisition) obtained were converted to PCR file format (Phoenix CT Reconstruction) via a reconstruction step and three-dimensional and cross-sectional images of sample were investigated using VG Studio Max (v.2.1) software. Morphology and chemical composition of the corrosion products on the surface of samples were analyzed by scanning electron microscopy (SEM) (SU8000, Hitachi, Japan) after ion beam coating. Cross-section samples for SEM analyses were orthogonally cut using a sectioning machine (TechCut 5TM, Allied High Tech Products Inc., USA) after mounting the sample in epoxy resin (Epokwick® Epoxy resin, Buehler, USA). The thickness of the general corrosion product was measured using SEM images of cross-section samples and the depth of localized corrosion was measured using micro-CT data. Average values and standard deviations were determined after measuring 10 times for each sample. X-ray diffraction (XRD) patterns were obtained using a D8 Discover X-ray diffractometer (Bruker AXS GmbH, Germany) equipped with CuK_{α1} radiation source (wavelength λ = 1.5406 Å). The operating voltage and current were 40 kV and 40 mA, respectively, and the step size and speed were 0.01426° per step and 0.3 s per step in the 2θ range 10–80°.

3. Results

Immersion tests were carried out in the various solutions to monitor corrosion in the initial stage for 1 day at 37 °C and to

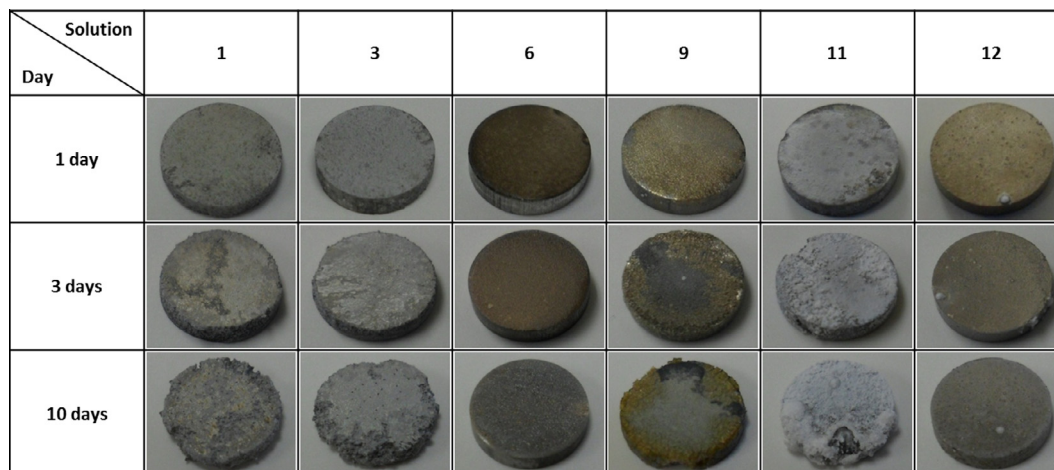


Fig. 1. Optical images of corroded AZ31B after immersion tests in solution.

observe more long-term effects due to the process of corrosion at 37 °C for 3 and 10 days, respectively.

Fig. 1 shows optical images of alloy AZ31B after immersion in solutions for 1, 3 and 10 days. The color of the two samples immersed in solutions 1 and 3 changed from a glossy surface to gray, and localized corrosion was observed on a small portion of the edge on day 1, which spread to the central part of the surface over the course of immersion. In the case of the sample tested in solution 6 the surface was covered with a brown film within 1 day, the color changing to dark gray after immersion for 10 days as the film thickened. Localized corrosion was only found on the surface after immersion in solution 6 for 10 days. The surface of the sample immersed in solution 9 was bright brown in the initial stages, changing to gray gradually with immersion time. White calcium phosphate was deposited on the surface of the sample tested in solution 11 within 1 day, and the thickness of precipitate increased with prolonged immersion. Its growth rate around the edges was faster than centrally and significant localized corrosion occurred in one place where the thick precipitate had detached from the surface. In the case of the sample tested in solution 12, the color changed from brown to gray over the 10 day time course, and only a few small corrosion products were found on the surface without significant localized corrosion.

The variations in pH during the immersion tests ($n = 3$) in each solution are shown in Fig. 2. The pH of solutions 1–4 increased up to 9.9 with an average daily increment of about 2.1. The pH of solution 5 showed a tendency to increase in magnitude over the 10 day course of the experiments. In the case of solutions 6 and 7 there was little change in pH, with an average daily pH increment of less than 0.1. In the case of the addition of small amounts of HCO_3^- , as with solution 8, the average daily increment was about 1.7. As the amount of HCO_3^- was increased the average daily increment decreased by about 40% compared with solution 8. In the case of solution 11 the solution pH was lower than before the immersion test, with an average daily decrease for solution 11 of about 0.4. The pH variation of solution 11 without AZ31B sample was tested to confirm that the decrease in pH was due to dissolution of CO_2 from the atmosphere, resulting in an average daily decrease of about 0.1. The average daily increment of solution 12, which included calcium, phosphate and carbonate ions, was about 0.5 and was between the average daily increments of solutions 6 and 9 including same amounts of phosphate and carbonate ions, respectively.

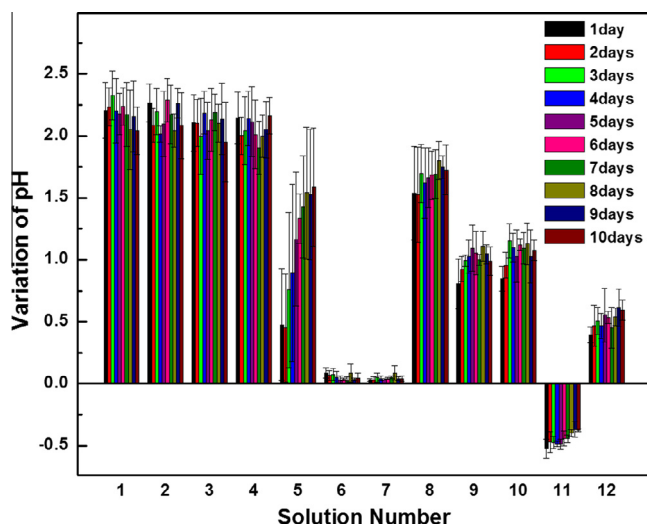


Fig. 2. Variations in pH during immersion tests in each solution containing various ions at various concentrations.

Figs. 3 and 4 show SEM images of the surface of AZ31B after immersion in the various solutions for 1 and 10 days, respectively. As shown in Fig. 3a, the majority of corrosion sites were along grain boundaries with small localized corrosion and nano-sized $\text{Mg}(\text{OH})_2$ films formed in the matrix after immersion in NaCl solution (1) for 1 day. The size of the $\text{Mg}(\text{OH})_2$ honeycomb film and localized corrosion increased with increasing immersion time (Fig. 4a). The morphology of the surface corroded in solution 2 containing calcium ions was similar to the morphology of the sample immersed in solution 1, with no distinguishing characteristics observed (Figs. 3b and 4b). A dense corrosion product with numerous micro-cracks spanning the whole of the surface was observed on the sample soaked for 1 day in solution 6 containing phosphate ions (Fig. 3c), which thickened over time (Fig. 4c). As shown in Fig. 3d, a thick and dense corrosion product composed of tiny styloid microstructures formed on the surface of the sample immersed for 1 day in solution 9 containing carbonate ions, the thickness of which increased with immersion time (Fig. 4d). Spherical calcium phosphate precipitates composed of plate-like microstructures were incompletely deposited on the surface of the sample immersed in solution 11 containing calcium and phosphate ions. As the globular precipitate grew larger the film became denser (see Figs. 3e and 4e). On adding carbonate ions in solution with calcium and phosphate ions (solution 12) the corrosion characteristics were completely changed compared with the surface corrosion in solution 11. The surface was covered with dense corrosion products with spherical calcium phosphate deposits partially formed at sites where pitting corruptions occurred after immersion in solution 12 for 1 day (Fig. 3f). The film became thicker as time passed (Fig. 4f).

Table 2 shows the chemical composition of general corrosion products formed on the surface after immersion tests in solutions that had ion concentrations relevant to human plasma [22] for 10 days as detected by EDX analysis. The predominant constituents formed on the AZ31B surface after immersion in solutions 1 and 3 for 1 and 10 days were O and Mg, and the amount of O in the corrosion product increased significantly. It is noteworthy that calcium was barely detected in corrosion products formed in solution 3, which had an identical calcium ion concentration to human plasma. The primary components of the corrosion products generated in solution 6 were O, Mg and P, suggesting the presence of tertiary magnesium phosphate. The constituents of the corrosion products created in solution 9 in 1 day were similar to those of the corrosion products formed in solution 1 after 10 days, except for the aluminum signal (Fig. 5d) due to the rapid corrosion rate in the early stages. The component ratio scarcely changed after immersion for 10 days. The relative amount of Al detected in the corrosion product was larger than that predicted based on the composition of the AZ31B matrix and the corrosion product formed in solution 1. Also, the amount of carbon in the corrosion products formed in solutions 1 and 9 showed little difference despite solution 9 containing HCO_3^- ions. The principle components of the precipitate deposited from solution 11 on the surface of AZ31B after 1 day and 10 days were O, P and Ca. The Ca/P ratio was about 1.7–1.8. Magnesium was barely detected in the product, unlike the corrosion products formed in the other solutions. Thus it might be inferred from Table 2 and Fig. 5 that this product was only deposited on the surface and is not a corrosion product. The constituents of the corrosion products created in solution 12 were O, Mg, P and Ca, with a Ca/P ratio of about 0.8–1. The amount of Mg was higher and the Ca/P ratio lower than for the corrosion product formed in solution 11. The amount of Al in the corrosion product, in common with the corrosion product formed in solution 9, was greater than in corrosion products created in solutions without HCO_3^- ions.

Elemental mapping images of sample cross-sections (Fig. 5) show the predominant constituents of corrosion products formed

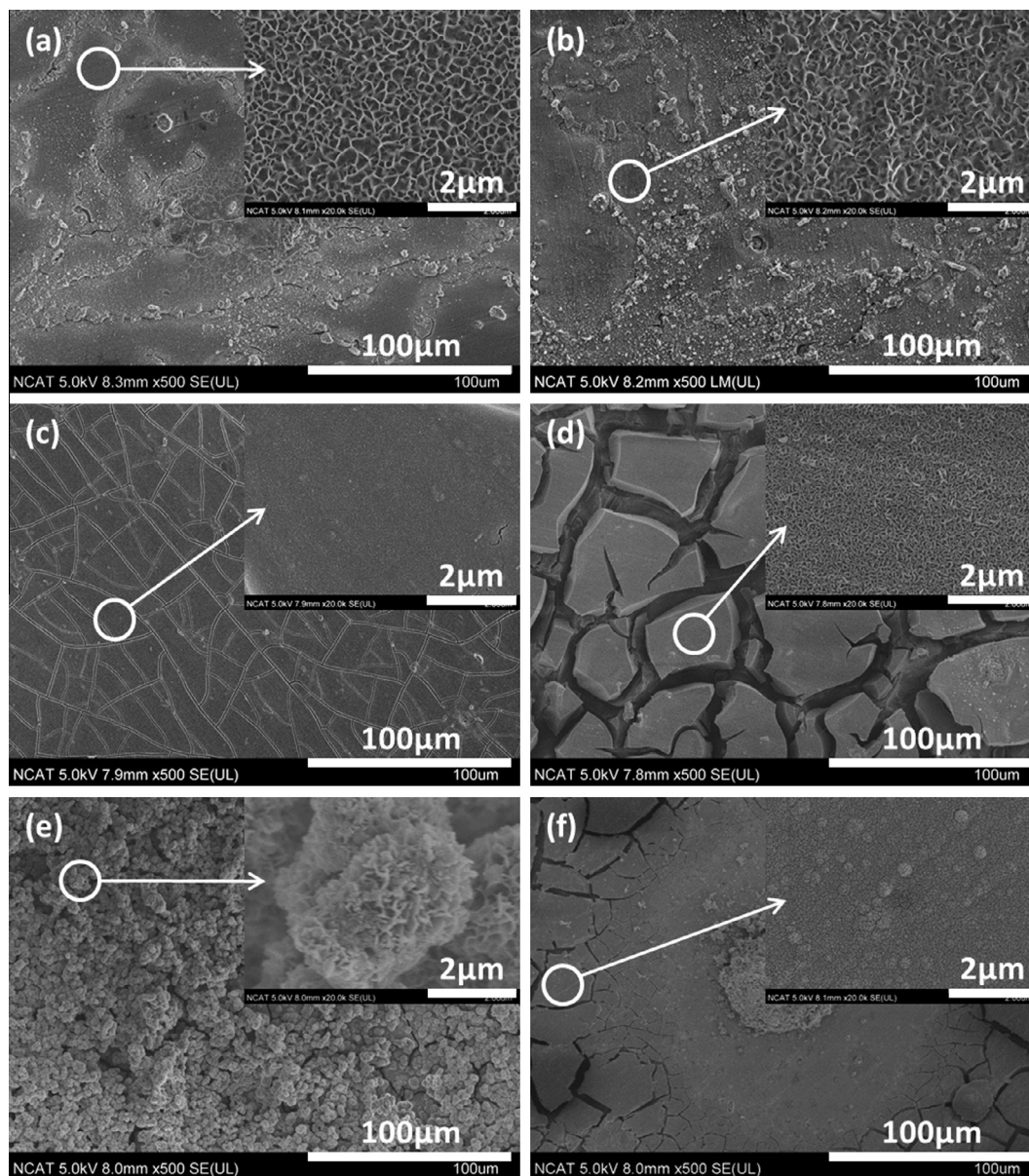


Fig. 3. SEM images of corroded surfaces after immersion tests in solution for 1 day. (a) Solution 1; (b) solution 3; (c) solution 6; (d) solution 9; (e) solution 11; (f) solution 12.

after immersion for 10 days in solution. As shown in Fig. 5d and f, the content of aluminum in the corrosion products formed in solutions containing HCO_3^- , such as solutions 9 and 12, was greater than that of Al (2.91 at.%) confirmed in the matrix of alloy AZ31B as determined from the EDX data in Table 2. A greater amount of calcium was present in the top than bottom layer of corrosion products formed in solution 12, while calcium and phosphate were uniformly distributed in the precipitate formed in solution 11. This result was confirmed by a line analysis, as shown in Fig. 6.

Fig. 7 shows CT images of samples after immersion in the solutions for 10 days. Fig. 7a and b shows similar features of corrosion on the samples immersed in solutions 1 and 3 for 10 days. Localized corrosion penetrated deeply into the matrix near the edge of both samples, and significant amounts of matrix were completely degraded. Small corrosion pits were uniformly observed across the whole of the surface of the samples, and voids created by dissolution of the matrix were observed just below the sites where pitting corrosion occurred. No localized corrosion was found on the surface tested in solution 6, and thin and dense corrosion prod-

ucts formed on the surface (Fig. 7c). A thick layer of corrosion products was uniformly formed on the surface of the sample immersed in solution 9 for 10 days, and the corrosion products penetrated deep into the matrix (Fig. 7d). In the case of the sample tested in solution 11 for 10 days calcium phosphate was deposited on the surface without pitting corrosion, except for one area where severe localized corrosion occurred in a place where the thick precipitate became detached (Fig. 7e). As shown in Fig. 7f, the sample immersed in solution 12 for 10 days was uniformly corroded without severe localized corrosion. Some voids and corrosion products formed by low level pitting corrosion were observed on the surface.

Fig. 8 shows the thicknesses of the corrosion products and precipitates and the depths of corrosion pitting formed on samples after immersion tests in each solution containing various ions at various concentrations for 10 days. The thicknesses and depths of corrosion products were measured on SEM images and using CT data. The thicknesses of the corrosion products and depths of pitting corrosion measured in samples immersed in solutions

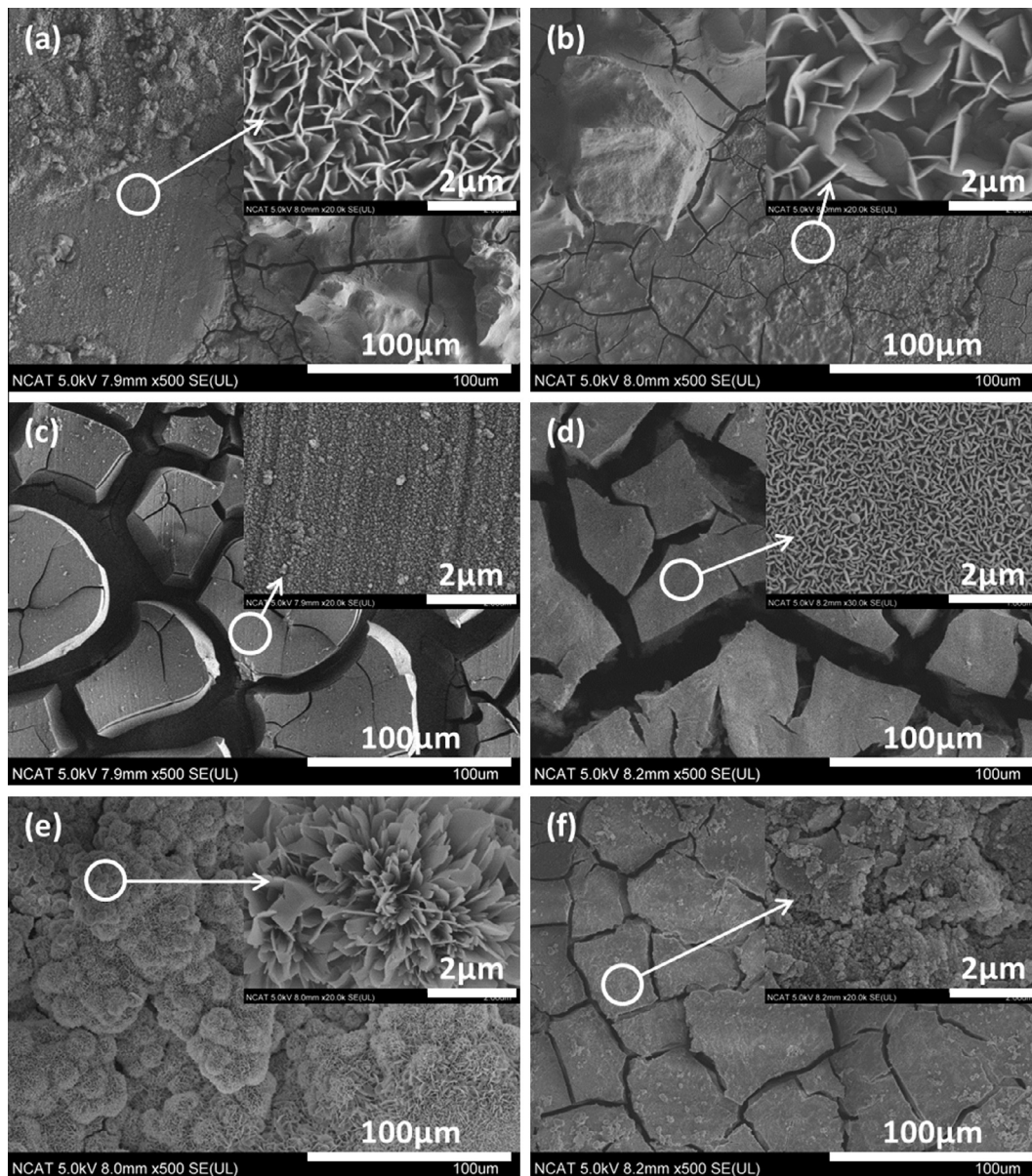


Fig. 4. SEM images of corroded surfaces after immersion tests for 10 days. (a) Solution 1; (b) solution 3; (c) solution 6; (d) solution 9; (e) solution 11; (f) solution 12.

Table 2

Chemical compositions of corrosion products formed on the surface after immersion tests in solution for 1 and 10 days detected by EDX analysis (at.%).

Solution	Immersion time	C	O	Na	Mg	Al	P	Cl	Ca	Zn
1	1 day	10.12	28.51	0.54	58.64	1.95		0.00		0.23
	10 days	4.15	63.12	0.48	30.50	1.70		0.06		0.00
3	1 day	6.55	37.50	0.40	52.45	1.90		0.74	0.13	0.33
	10 days	4.80	62.85	0.00	29.25	3.05		0.05	0.00	0.00
6	1 day	4.28	54.26	0.41	30.28	1.67	8.68	0.00		0.41
	10 days	7.50	69.49	0.35	15.18	2.74	3.94	0.04		0.76
9	1 day	6.89	69.96	0.11	17.78	4.54		0.16		0.57
	10 days	9.72	69.29	0.09	16.16	4.23		0.06		0.44
11	1 day	3.67	60.11	0.18	0.22	0.00	12.49	0.00	23.32	0.00
	10 days	2.31	63.32	0.59	0.32	0.23	12.32	0.00	20.69	0.23
12	1 day	4.94	62.48	0.11	17.22	4.64	5.91	0.00	4.51	0.21
	10 days	4.73	62.01	0.34	10.00	4.40	8.80	0.09	8.97	0.67

containing calcium salts (solution 2–4) for 10 days were similar to the value for the sample immersed in NaCl solution (solution 1). In the case of samples tested in solutions including phosphate salts

general and pitting corrosion of the sample tested in solution 5 were decreased compared with the values for the sample immersed in solution 1. Pitting corrosion was not observed on the

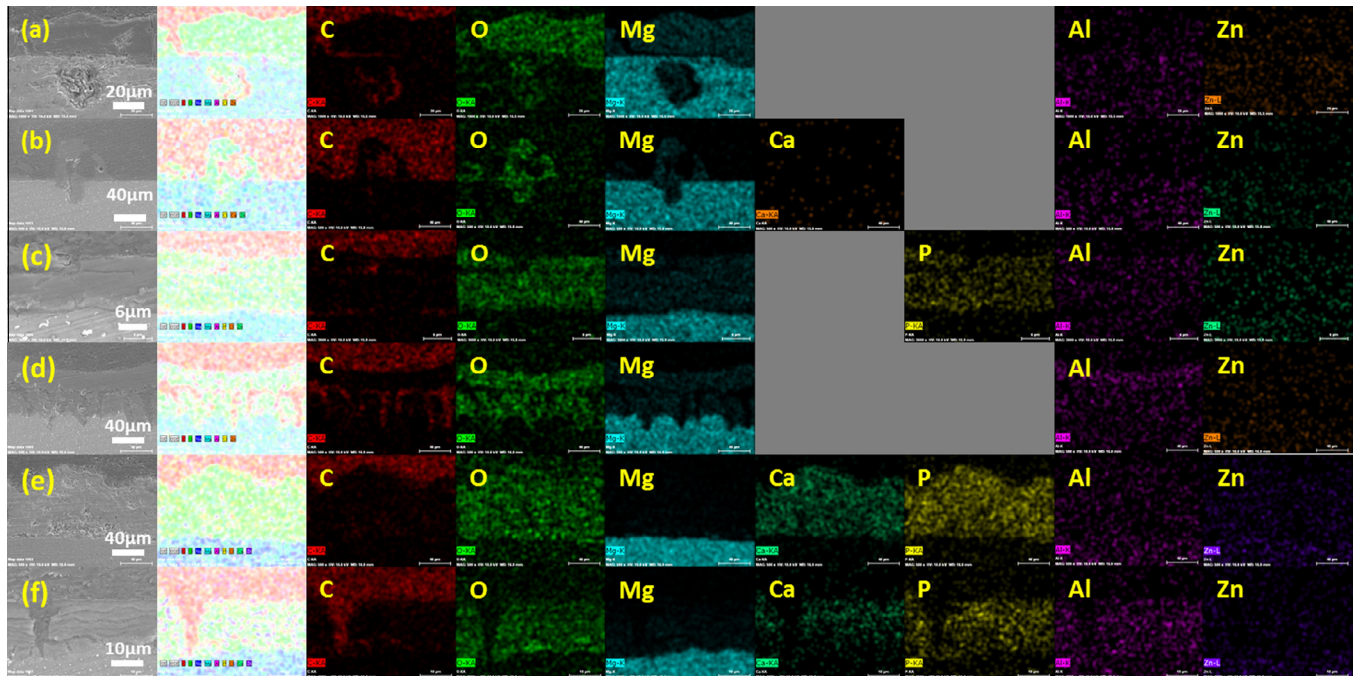


Fig. 5. EDX mapping data of cross-sections of corrosion products after immersion tests in solution for 10 days. (a) Solution 1; (b) solution 3; (c) solution 6; (d) solution 9; (e) solution 11; (f) solution 12.

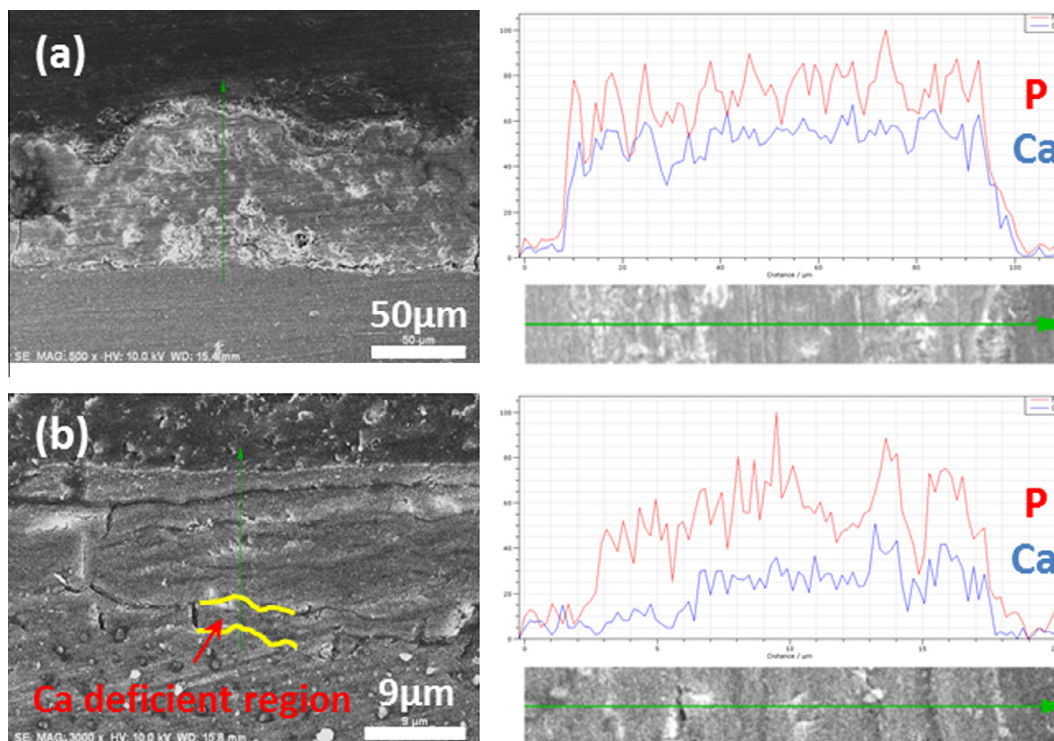


Fig. 6. Line analysis of cross-sections of corrosion products after immersion tests in solution for 10 days. (a) Solution 11; (b) solution 12.

surface of samples immersed in solutions 6–7. The corrosion properties of the sample tested in solution 8, with a low concentration of carbonate ions, was similar to the result for the sample tested in solution 1. However, as the concentration of HCO_3^- ions was increased more general corrosion progressed. No general corrosion products or pitting corrosion were observed on the surface of the sample tested in solution 11, which included calcium and phos-

phate ions. Coupled with the EDX results, it appears that only calcium phosphate was deposited on the surface. The thickness of the general corrosion products and the depth of pitting corrosion for the sample immersed in solution 12 were greater than those of the sample in solution 6 with the same concentrations of HPO_4^{2-} ions, and were lower than those of the sample tested in solution 9 with the same concentration of HCO_3^- ions.

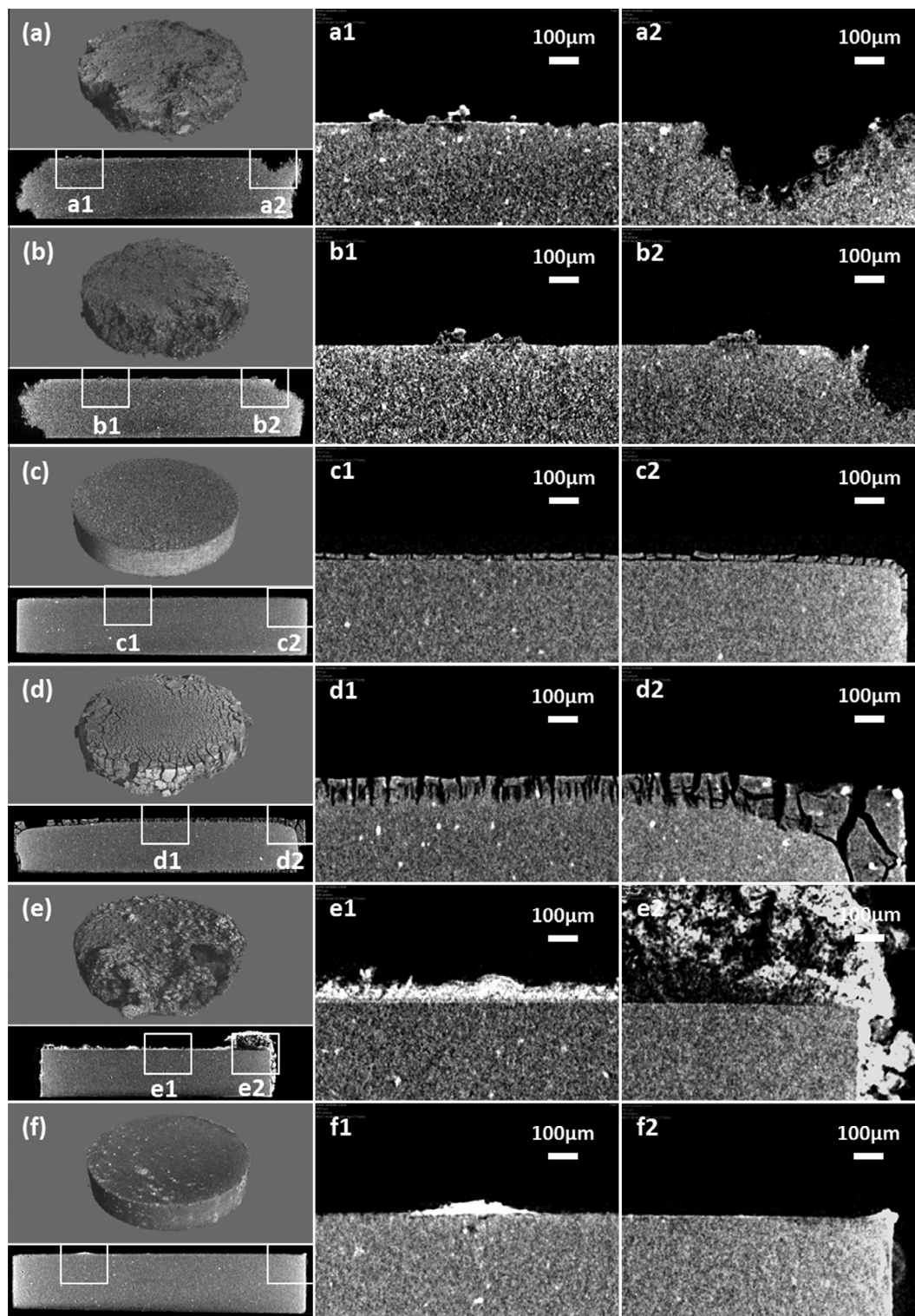


Fig. 7. CT images of samples after immersion tests in solution for 10 days. (a) Solution 1; (b) solution 3; (c) solution 6; (d) solution 9; (e) solution 11; (f) solution 12.

Fig. 9 shows XRD patterns collected for alloy AZ31B and the corrosion products after immersion in each solution containing various ions at various concentrations for 10 days. In addition to the Mg peaks observed for an AZ31B sample before immersion, brucite ($\text{Mg}(\text{OH})_2$) and a hydrotalcite (HT)-like compound ($[\text{Mg}_{0.833}\text{Al}_{0.167}(\text{OH})_2](\text{CO}_3)_{0.083}\cdot 0.75\text{H}_2\text{O}$) were identified on samples after immersion in solutions 1 and 3 for 10 days. The peaks associated with the HT-like compound along with the Mg peaks were present

in the case of the sample immersed in solution 9 for 10 days, at intensities above those of the samples tested in solution 1 and 3, however, no brucite peaks were observed. No additional peaks other than those associated with Mg were observed on the sample immersed in solution 6 even though P was detected by EDX, as shown Table 2. The peaks identified on the sample immersed in solution 11 were mainly octacalcium phosphate (OCP) ($\text{Ca}_8\text{H}_2(\text{PO}_4)_6\cdot 5\text{H}_2\text{O}$) and hydroxyapatite (HAp) ($\text{Ca}_{10}(\text{PO}_4)_6(\text{OH})_2$),

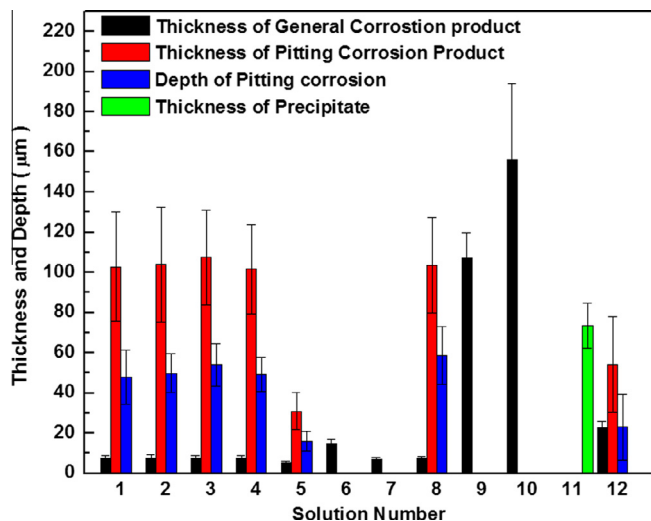


Fig. 8. Thicknesses of corrosion products and precipitates formed on and depths of pitting corrosion in samples after immersion tests in each solution containing various ions at various concentrations for 10 days.

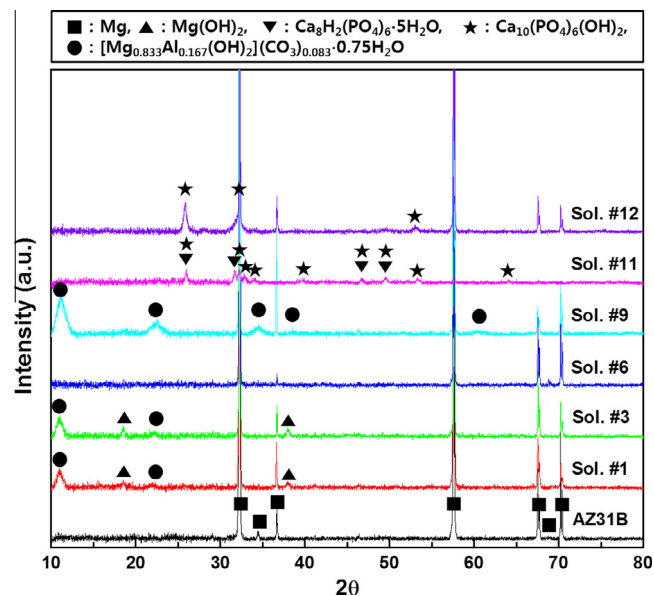


Fig. 9. XRD patterns of corrosion products after immersion tests in solution for 10 days.

and Mg peaks were not observed. However, only those peaks associated with HAp and Mg were observed on the sample tested in solution 12.

4. Discussion

In this study the effects of physiologically relevant salts on the corrosion behavior of magnesium alloy AZ31B were investigated individually at concentrations close to the physiological concentration and in also combination. Assessment tools included variations in pH, observations of the morphology and cross-sections by SEM and micro-CT, and comparisons of the chemical components using EDX and XRD analysis of corrosion products after immersion tests. The main corrosion mechanisms of alloy AZ31B in solutions including chloride (solution 1) or chloride and calcium ions (solutions 2–4) are localized corrosion and uniform corrosion, as confirmed in Figs. 7

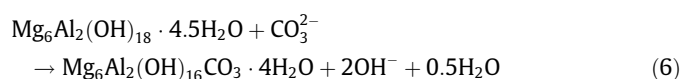
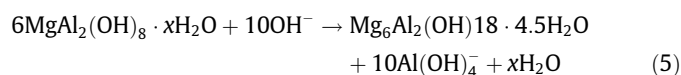
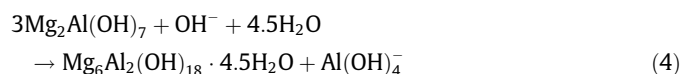
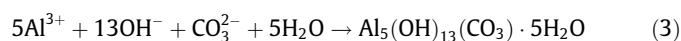
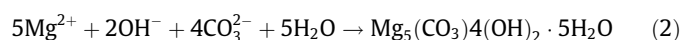
and 8. The corrosion products were mainly $\text{Mg}(\text{OH})_2$ and $[\text{Mg}_{0.833}\text{Al}_{0.167}(\text{OH})_2](\text{CO}_3)_{0.083}\cdot 0.75\text{H}_2\text{O}$, as shown in Fig. 9. HT is a hydroxycarbonate of magnesium that has the typical chemical formula $\text{Mg}_6\text{Al}_2(\text{OH})_{16}\text{CO}_3\cdot 4\text{H}_2\text{O}$ and has a layered crystal structure which consists of positively charged brucite-like layers $(\text{Mg}_6\text{Al}_2(\text{OH})_{16})^{2+}$ and negatively charged interlayers $(\text{CO}_3\cdot 4\text{H}_2\text{O})^{2-}$ [23–25]. HT-like compounds (HTLcs) are similar to HT and are represented by the general formula $[\text{M}^{\text{II}}_{1-x}\text{M}^{\text{III}}_x(\text{OH})_2]^{x+}\cdot [\text{A}^{n-}]_{x/n}\cdot m\text{H}_2\text{O}$, where M^{II} and M^{III} are divalent and trivalent metals, respectively, A^{n-} is a n -valent anion, and the $\text{M}^{\text{II}}/\text{M}^{\text{III}}$ ratio is $(1-x)/x$ [24,26]. Many studies on the structural and chemical properties as well as mechanisms of formation and decomposition of these HT and HTLcs have been reported [23,24,27,28]. Their presence in the corrosion products or conversion films formed on Mg–Al alloys in various corrosive environments has been verified by several researchers, and it has been established in the literature that they improve the corrosion resistance of Mg alloys in aggressive environments [25,26,29–33].

The corrosion rate of magnesium increased with increasing HCO_3^- concentration [34]. Pardo et al. [35] reported that the main corrosion product formed on the surface of some Mg–Al alloys in NaCl solution was brucite ($\text{Mg}(\text{OH})_2$), with evidence of magnesite ($\text{MgCO}_3\cdot 2\text{H}_2\text{O}$) due to dissolution of CO_2 in the atmosphere was found using XRD. The variation of pH increment for 10 day was not observed even though pH increased considerably after 1 day in this study. The pH of solution 1 in Fig. 2 show that pH was increased up to 9.9 with an average daily increment of about 2.1. This may be caused by chloride ions and galvanic reaction, as although $\text{Mg}(\text{OH})_2$ is formed on the surface in NaCl solution it can be converted into the more soluble MgCl_2 [36]. Additionally, the intermetallic phase in alloy AZ31B can cause the formation of a microgalvanic couple at grain boundaries between the secondary phase and primary Mg matrix. These reactions make the surface of magnesium alloys more active and accelerate corrosion in NaCl solution.

No effect of calcium on corrosion behavior was observed in this study, in agreement with a related study [13] in which phosphates were deposited without calcium, but calcium could be only precipitated in the form of calcium phosphate when phosphate and calcium were present together. The presence of $\text{Mg}(\text{OH})_2$ on the surface without the presence of Ca^{2+} ions, as determined by EDX and XRD measurements, can be explained by the equilibrium solubility constants of the metal hydroxides. The K_{sp} value at 25 °C for $\text{Mg}(\text{OH})_2$ is 5.61×10^{-12} and that for $\text{Ca}(\text{OH})_2$ is 5.02×10^{-6} . $\text{Ca}(\text{OH})_2$ is more soluble than $\text{Mg}(\text{OH})_2$ and little or no Ca^{2+} salts precipitate. The cation solubility effect is reversed for phosphate ions, specifically in that the K_{sp} for $\text{Ca}_3(\text{PO}_4)_2$ is 2.07×10^{-33} and the K_{sp} for $\text{Mg}_3(\text{PO}_4)_2$ is 1.04×10^{-24} . Thus Ca^{2+} is more likely to be detected as the phosphate salt than is Mg^{2+} on top of the surface of corroding magnesium substrates [20].

The small variations in pH increment in solutions containing HPO_4^{2-} may be attributed to several factors: the consumption of OH^- induced by dissolution of Mg when $\text{Mg}_3(\text{PO}_4)_2$ was formed on the surface by chemical reaction with HPO_4^{2-} in solution [18], retarding the dissolution of Mg due to formation of stable dense $\text{Mg}_3(\text{PO}_4)_2$ on the surface, and the buffering effect of phosphate. The Mg/P atomic ratio in our experiment was 3.85 according to the EDX results in Table 2, which is higher than the expected Mg/P atomic ratio of 1.5 suggested by the formula $\text{Mg}_3(\text{PO}_4)_2$. The presence of $\text{Mg}(\text{OH})_2$ as a corrosion product along with $\text{Mg}_3(\text{PO}_4)_2$ would account for this observation [37]. However, the XRD peaks of $\text{Mg}_3(\text{PO}_4)_2$ and $\text{Mg}(\text{OH})_2$ cannot be observed in Fig. 9, even though P was detected by EDX. Thus the corrosion products composed of $\text{Mg}_3(\text{PO}_4)_2$ and $\text{Mg}(\text{OH})_2$ formed in solutions containing HPO_4^{2-} may be amorphous and not crystalline [13]. The many micro-cracks observed in the SEM images (Figs. 3c and 4c) are probably produced due to dehydration of the corrosion products during the samples preparation process for SEM [18].

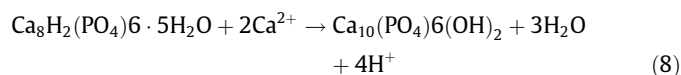
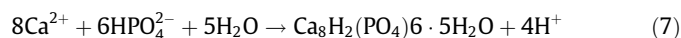
The reduced pH increment in solutions containing carbonate ions may be attributable to the consumption of OH^- by HCO_3^- [38], the formation of HT [30,31], and the buffering effect of carbonate [39]. The consumption of OH^- by HCO_3^- (Eq. (1)) and the formation of HT (Eq. (2)–(6)) can occur by the following set of reactions [30,31,38].



A possible mechanism of formation of HT on the AZ31B alloy was systematically organized and proposed by Chen et al. [31] as follows: (i) formation of metastable hydrous carbonate (Eqs. (2) and (3)); (ii) decomposition of the carbonate to form the precursors of HT, which are Al-rich compounds, replacing of Mg^{2+} or Al^{3+} ; (iii) dissolution of Al^{3+} from the precursor (Eqs. (4) and (5)); (iv) exchange of OH^- for CO_3^{2-} .

Thick and uniform corrosion products composed of $[\text{Mg}_{0.833}\text{-Al}_{0.167}(\text{OH})_2](\text{CO}_3)_{0.083} \cdot 0.75\text{H}_2\text{O}$, not $\text{Mg}(\text{OH})_2$, were observed on the surface of Mg alloy AZ31B immersed in solutions containing carbonate in this study. Xin et al. [18] asserted that HCO_3^- in solution accelerated the initial corrosion of magnesium but retarded pitting corrosion and the corrosion rate in the long-term, due to formation of a passivation layer consisting of magnesium carbonate.

It is interesting that the pH decreased in solution 11, which included both calcium and phosphate ions, as shown Fig. 2. The pH usually increases during immersion tests of magnesium alloys because H_2 and OH^- are generated at both the anode and cathode as magnesium is corroded [36]. The reason for the pH decrement in solution 11 may be the formation of OCP or the transformation of OCP to HAp on the surface of alloy AZ31B, as confirmed by the XRD data (Fig. 9). These two processes increase the hydrogen ion concentration, as shown in the following two chemical reactions [40,41].



However, in the case of solution 12 an increase in pH was observed, which means that the rate of corrosion of the magnesium alloy in the presence of carbonate was faster than the formation of HAp in the presence of calcium and phosphate, as in solution 11. Our results show that the corrosion product morphology and composition varied with solution pH when HAp (high pH) and OCP (low pH) were formed, consistent with a similar reported study [42]. The plate-like microstructures in the rosette clusters of OCP and HAp in Figs. 3 and 4e have been observed in many previous studies [42–44] of calcium phosphate coatings on titanium and magnesium alloys and in in vitro and in vivo tests for them in SBFs. Reiner et al. [45] proposed a three stage mechanism: (1)

precipitation of OCP; (2) hydrolysis of OCP to Ca-deficient HAp; (3) OCP crystal growth, which initiates under low calcium ion concentration and pH conditions. Typically Ca/P atomic ratios can be used to determine the nature of a particular calcium phosphate phase: anhydrous calcium phosphate (CaHPO_4) and calcium phosphate dehydrate ($\text{CaHPO}_4 \cdot 2\text{H}_2\text{O}$) = 1.0; OCP ($\text{Ca}_8\text{H}_2(\text{PH}_4)_6 \cdot 5\text{H}_2\text{O}$) = 1.33, tricalcium phosphate ($\text{Ca}_3(\text{PO}_4)_2$) = 1.5; HAp ($\text{Ca}_{10}(\text{PO}_4)_6(\text{OH})_2$) = 1.67 [46]. Using the results of EDX (Table 2) and XRD (Fig. 9) we could confirm that the calcium phosphate phases formed on the surface in solution 11 were OCP and HAp. The corrosion products formed in solution 12 were identified as HAp from the XRD patterns, but we could not precisely determine the cause of the low Ca/P ratio and the high concentration of aluminum in the corrosion product. We hypothesize that the cause may be the presence of magnesium apatite ($\text{Ca}_{0.86}, \text{Mg}_{0.14}$) (PO_4)₆(OH)₂[47] and a small quantity of HTLcs.

Two particular noteworthy phenomena were observed in this study. Firstly, as shown in Fig. 5, the amount of aluminum was relatively greater in the corrosion products in solutions 9 and 12 than in the matrix of AZ31B and the corrosion products formed in other solutions. Secondly, more calcium was present in the top layer than in the bottom layer of the corrosion products created in solution 12, which included calcium, phosphate and carbonate ions.

5. Conclusion

The primary corrosion products formed in NaCl solution were brucite and HTLcs. The corrosion behavior in NaCl solution with Ca^{2+} was similar to the corrosion behavior in NaCl solution. Corrosion resistance increased with increasing HPO_4^{2-} concentration, due to the formation of a stable passivation layer. A thick corrosion product layer of HTLc formed on the magnesium alloy surface on addition of HCO_3^- to the chloride solution. OCP and HAp formed when calcium and phosphate ions were in solution in the presence of the Mg alloy (AZ31B). In conclusion, we have found individual roles of the three constituents Ca^{2+} , HPO_4^{2-} , and HCO_3^- and their influence on the corrosion product layer during magnesium corrosion, and have gained an insight into the effect of combinations of these physiological salts when combined. It is hoped that these data and this analysis will be used in future studies to help elucidate the corrosion behavior of Mg alloys in vivo, and lead to better in vitro tests that are predictive of the in vivo behavior of magnesium.

Acknowledgements

This research was partially supported by the Engineering Research Center for Revolutionizing Metallic Biomaterials with a grant from the National Science Foundation. We appreciate the contributions of Dr. Frank Witte for proofreading the manuscript.

Appendix A. Figures with essential colour discrimination

Certain figures in this article, particularly Figs. 1, 2, 5, 6, 8 and 9 are difficult to interpret in black and white. The full colour images can be found in the on-line version, at <http://dx.doi.org/10.1016/j.actbio.2013.03.026>.

References

- [1] Hort N, Huang Y, Fechner D, Störmer M, Blawert C, Witte F, et al. Magnesium alloys as implant materials – principles of property design for Mg–RE alloys. *Acta Biomater* 2010;6:1714–25.
- [2] Hermawan H, Dubé D, Mantovani D. Degradable metallic biomaterials: design and development of Fe–Mn alloys for stents. *J Biomed Mater Res A* 2010;93A(2):1–11.

- [3] Velikokhatnyi OI, Kumta PN. First-principles studies on alloying and simplified thermodynamic aqueous chemical stability of calcium-, zinc-, aluminum-, yttrium- and iron-doped magnesium alloys. *Acta Biomater* 2010;6:1698–704.
- [4] Witte F, Fischer J, Nellesen J, Crostack HA, Kaese V, Pisch A, et al. In vitro and in vivo corrosion measurements of magnesium alloys. *Biomaterials* 2006;27:1013–8.
- [5] Witte F, Hort N, Vogt C, Cohen S, Kainer KU, Willumeit R, et al. Degradable biomaterials based on magnesium corrosion. *Curr Opin Solid State Mater Sci* 2008;12:63–72.
- [6] Feyerabend F, Drücker H, Laipple D, Vogt C, Stekker M, Hort N, et al. Ion release from magnesium materials in physiological solutions under different oxygen tensions. *J Mater Sci Mater Med* 2012;23:9–24.
- [7] Yun Y, Dong Z, Lee N, Liu Y, Xue D, Guo X, et al. Revolutionizing biodegradable metals. *Mater Today* 2009;12:22–32.
- [8] Song G, Atrens A, Stjohn D, Nairn J, Li Y. The electrochemical corrosion of pure magnesium in 1 N NaCl. *Corros Sci* 1997;39(5):855–75.
- [9] Jönsson M, Persson D, Thierry D. Corrosion product formation during NaCl induced atmospheric corrosion of magnesium alloy AZ91D. *Corros Sci* 2007;49:1540–58.
- [10] Abidin NIZ, Martin D, Atrens A. Corrosion of high purity Mg, AZ91, ZE41 and Mg₂Zn_{0.2}Mn in Hank's solution at room temperature. *Corros Sci* 2011;53:862–72.
- [11] Waizy H, Weizbauer A, Moderjewski C, Witte F, Windhagen H, Lucas et al. A. In vitro corrosion of ZEK100 plates in Hank's balanced salt solution. *BioMedical Engineering Online* 2012;11/12:1–14; <http://www.biomedical-engineering-online.com/content/11/1/12>.
- [12] Xin Y, Liu C, Zhang X, Tang G, Tian X, Chu PK. Corrosion behavior of biomedical AZ91 magnesium alloy in simulated body fluids. *J Mater Res* 2007;22(7):2004–11.
- [13] Rettig R, Virtanen S. Composition of corrosion layers on a magnesium rare-earth alloy in simulated body fluids. *J Biomed Mater Res A* 2009;88A(2):359–69.
- [14] Wang Y, Wei M, Gao J, Hu J, Zhang Y. Corrosion process of pure magnesium in simulated body fluid. *Mater Lett* 2008;62:2181–4.
- [15] Carboneras M, García-Alonso MC, Escudero ML. Biodegradation kinetics of modified magnesium-based materials in cell culture medium. *Corros Sci* 2011;53:1433–9.
- [16] Willumeit R, Fischer J, Feyerabend F, Hort N, Bismayer U, Heidrich S, et al. Chemical surface alteration of biodegradable magnesium exposed to corrosion media. *Acta Biomater* 2011;7:2704–15.
- [17] Wang L, Shinohara T, Zhang BP. Influence of chloride, sulfate and bicarbonate anions on the corrosion behavior of AZ31 magnesium alloy. *J Alloys Compd* 2010;496:500–7.
- [18] Xin Y, Huo K, Tao H, Tang G, Chu PK. Influence of aggressive ions on the degradation behavior of biomedical magnesium alloy in physiological environment. *Acta Biomater* 2008;4:2008–15.
- [19] Gulbrandsen E. Anodic behavior of Mg in HCO₃⁻/CO₃²⁻ buffer solution. Quasi-steady measurements. *Electrochim Acta* 1992;37(8):1403–12.
- [20] Yamamoto A, Hiromoto S. Effect of inorganic salts, amino acids and proteins on the degradation of pure magnesium in vitro. *Mater Sci Eng C* 2009;29:1559–68.
- [21] Heikal FET, Fekry AM, Fatayerji MZ. Electrochemical behavior of AZ91D magnesium alloy in phosphate medium – part I. Effect of pH. *J Appl Electrochem* 2009;39:583–91.
- [22] Gamble JE. *Chemical anatomy, physiology and pathology of extracellular fluid*. Cambridge, MA: Harvard University Press; 1967. p. 1–17.
- [23] Miyata S. Anion-exchange properties of hydrotalcite-like compounds. *Clays Clay Miner* 1983;31(4):305–11.
- [24] Trave A, Selloni A, Goursot A, Tichit D, Weber J. First principles study of the structure and chemistry of Mg-based hydrotalcite-like anionic clays. *J Phys Chem B* 2002;106:12291–6.
- [25] Lin JK, Hsia CL, Uan JY. Characterization of Mg, Al-hydrotalcite conversion film on Mg alloy and Cl⁻ and CO₃²⁻ anion-exchangeability of the film in a corrosive environment. *Scripta Mater* 2007;56:927–30.
- [26] Chen J, Song Y, Shan D, Han EH. Study of the corrosion mechanism of the in situ grown Mg–Al–CO₃²⁻ hydrotalcite film on AZ31 alloy. *Corros Sci* 2012;65:268–77.
- [27] Bellotto M, Rebours B, Clause O, Lynch J. A reexamination of hydrotalcite crystal chemistry. *J Phys Chem* 1996;100:8527–34.
- [28] Bellotto M, Rebours B, Clause O, Lynch J. Hydrotalcite decomposition mechanism: a clue to the structure and reactivity of spinel-like mixed oxides. *J Phys Chem* 1996;100:8535–42.
- [29] Lindström R, Svensson JE, Johansson LG. The influence of carbon dioxide on the atmospheric corrosion of some magnesium alloys in the presence of NaCl. *J Electrochem Soc* 2002;149(4):B103–7.
- [30] Chen J, Song Y, Shan D, Han EU. In situ growth of Mg–Al hydrotalcite conversion film on AZ31 magnesium alloy. *Corros Sci* 2011;53:3281–8.
- [31] Chen J, Song Y, Shan D, Han EU. Study of the in situ growth mechanism of Mg–Al hydrotalcite conversion film on AZ31 magnesium alloy. *Corros Sci* 2012;63:148–58.
- [32] Merino MC, Pardo A, Arrabal R, Merino S, Casajús P, Mohedano M. Influence of chloride ion concentration and temperature on the corrosion of Mg–Al alloys in salt fog. *Corros Sci* 2010;52:1696–704.
- [33] Mathieu S, Rapin C, Steinmetz J, Steinmetz P. A corrosion study of the main constituent phases of AZ91 magnesium alloys. *Corros Sci* 2003;45:2741–55.
- [34] Baril G, Pèbère N. The corrosion of pure magnesium in aerated and deaerated sodium sulphate solutions. *Corros Sci* 2001;43:471–84.
- [35] Pardo A, Merino MC, Coy AE, Viejo F, Arrabal R, Feliú SJ. Influence of microstructure and composition on the corrosion behavior of Mg/Al alloys in chloride media. *Electrochimica Acta* 2008;53:7890–902.
- [36] Song G, Atrens A. Understanding magnesium corrosion; a framework for improved alloy performance. *Adv Eng Mater* 2003;5(12):837–58.
- [37] Su Y, Li G, Lian J. A chemical conversion hydroxyapatite coating on AZ60 magnesium alloy and its electrochemical corrosion behaviour. *Int J Electrochem Sci* 2012;7:11497–511.
- [38] Lindström R, Johansson LG, Svensson JE. The influence of NaCl and CO₂ on the atmospheric corrosion of magnesium alloy AZ91. *Mater Corros* 2003;54:587–94.
- [39] Lindström R, Johansson LG, Thompson GE, Skeldon P, Svensson JE. Corrosion of magnesium in humid air. *Corros Sci* 2004;46:1141–58.
- [40] Barrère F, Layrolle P, van Blitterswijk CA, De Groot K. Biomimetic calcium phosphate coating on Ti6Al4V: a crystal growth study of octacalcium phosphate and inhibition by Mg²⁺ and HCO₃⁻. *Bone* 1999;25(2):107S–11S.
- [41] Simmer JP, Fincham AG. Molecular mechanisms of dental enamel formation. *Crit Oral Biol Med* 1995;6:84–108.
- [42] Tomozawa M, Hiromoto S. Microstructure of hydroxyapatite- and octacalcium phosphate-coatings formed on magnesium by a hydrothermal treatment at various pH values. *Acta Mater* 2011;59:355–63.
- [43] Pietak A, Mahoney P, Dias GJ, Staiger MP. Bone-like matrix formation on magnesium and magnesium alloys. *J Mater Sci Mater Med* 2008;19:407–15.
- [44] Habibovic P, Li J, van der Valk CM, Meijer G, Layrolle P, van Blitterswijk CA, et al. Biological performance of uncoated and octacalcium phosphate-coated Ti6Al4V. *Biomaterials* 2005;26:23–36.
- [45] Reiner T, Gotman I. Biomimetic calcium phosphate coating on Ti wires versus flat substrates: structure and mechanism of formation. *J Mater Sci Mater Med* 2010;21:515–23.
- [46] Shadanbаз S, Dias GJ. Calcium phosphate coatings on magnesium alloys for biomedical applications: a review. *Acta Biomater* 2012;8:20–30.
- [47] Kuwahara H, Al-Abdullat Y, Mazaki N. Precipitation of magnesium apatite on pure magnesium surface during immersing in Hank's solution. *Mater Trans* 2001;42(7):1317–21.